Force/Stiffness Technique for Nondestructive Buckling Testing

Robert E. Jones* and Bruce E. Greene†
Boeing Aerospace Company, Seattle, Wash.

A plotting procedure is described which predicts local buckling and general instability loads nondestructively during testing. The method is shown to have a simple theoretical basis, and its relationship to the Southwell procedure is discussed. Typical forms of test data plots are cataloged and described, and procedures for application of the method are outlined. The procedure has been used extensively over the past two years with good results. Examples showing applications to combined load testing of beaded and tubular panels, and to proof testing of externally pressurized domes, are described and test data are given. Experience regarding instrumentation, procedural details, and accuracy of the method is discussed.

Introduction

THE prediction of buckling strengths of structural components by nondestructive testing has historically proved to be a difficult problem. Approaches to the problem are generally classifiable in the basic categories of data plotting schemes, vibration frequency extrapolation schemes, and methods based on measuring and extrapolating local structural stiffness. The best known example of the first category is Southwell's method, which has been successful for classical buckling of simple structures. For complex buckling behavior, Southwell's method has proved difficult to apply. A data plotting scheme presented by Galletly and Reynolds[1] was shown to offer considerable promise. This scheme is similar to the one proposed by the authors. Vibration frequency methods, which are extrapolation schemes based on the fact of zero frequency at the buckling load, have important drawbacks for complex problems. They fail to identify local modes, crippling and inelastic behavior, and encounter difficulties when buckling and vibration mode shapes are not closely related. Experience with these methods has been inconclusive.[2] A method based on local stiffness measurements made during primary load application, employing auxiliary loading devices, has been applied successfully in difficult problems.[3] This method appears to be the best of those currently available, at least for specimens not subject to creep. However, this method is costly, very slow in application, and requires access to the test specimen during loading.

The authors have worked with a nondestructive buckling test scheme of the data plotting type, using only basic test data consisting of load and strain (or displacement). The method quickly handles large amounts of test data, can be used with little or no delay in normal testing schedules and does not require access to the test specimens. With this method test specimens are usually instrumented thoroughly and large amounts of strain gage data are monitored in real time through the use of automatic data processing and data display techniques. This guards against undesired specimen failures due to local buckling or unanticipated general instability modes. The rapid processing capability is important to reduce testing cost and also to avoid difficulty with materials which might creep during delays in testing necessitated by extensive data review. Access to the test specimen is avoided because of safety considerations and also because of the need for testing at high temperatures, pressure, or other such environments. It appears that the method provides a much clearer understanding of complex buckling phenomena, and a quicker, more accurate failure load prediction than the Southwell procedure. The plotting variables are load vs load/strain. Since the first quantity is a force and the second is a stiffness, the procedure has been named the force/stiffness, or *F/S* method. Displacement can be used in place of strain, though loss of accuracy may result.

The need for such a nondestructive buckling test technique arose because of a planned study of buckling strengths of beaded and tubular panels for advanced aerospace vehicle applications. A goal of this work was to establish design data consisting of experimental interaction surfaces for buckling under combined loads of compression, shear, and lateral pressure. A large number of test panels would be required to establish such interaction surfaces by destructive testing. Furthermore, it was reasoned that differences in individual panels due to initial imperfections would cause scatter in the data that would obscure the true nature of the interaction surfaces. Therefore, a method was desired by which reliable buckling strength data could be obtained nondestructively from a single panel for different combinations of compression, shear, and lateral pressure loads.

The study of panel buckling strengths was sponsored by NASA Langley Research Center[4] under Contract NAS1-10749. A major part of the work under this contract consists of a large-scale testing program in which the *F/S* method has been applied successfully. The test results for beaded and tubular panels presented in this paper were derived from the above test program.

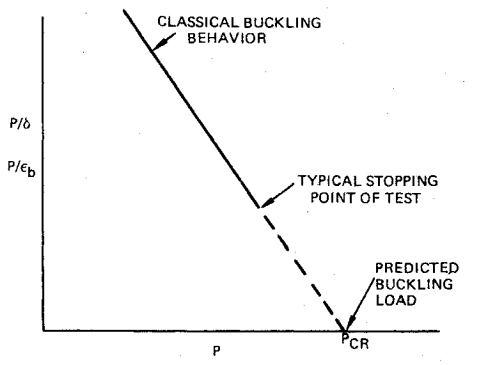

Fig. 1 Force stiffness plot for general instability.

Submitted April 15, 1974; presented as Paper 74-351 at the AIAA/ASME/SAE 15th Structures, Structural Dynamics and Materials Conference, Las Vegas, Nev., April 17-19, 1974; revision received April 30, 1975. The authors wish to express their thanks to G.A. Jensen for preparing the drafts of this paper, and to J. Bell, who directed the shell tests for the data pertaining to this work.

Index categories: Aircraft Structural, Design (including Loads); Aircraft Testing, (including Component Wind-Tunnel Testing); Structural Stability Analysis.

*Principal Engineer, Research and Engineering Division.

†Senior Specialist Engineer, Research and Engineering Division. Member AIAA.

Description of Method

The F/S method is a plotting procedure based on extrapolation. Two simple facts are the primary guides in its use: 1) for buckling behavior, data plotted in F/S format forms a straight or nearly straight line whose extension intersects the load axis at the critical buckling load; 2) a limiting strain level (yield or local crippling value) is represented in F/S format as a straight line through the origin, and intersection of this line by an F/S test curve signifies local failure.

In applications, most test data plot as curved lines, and extrapolations of these curves are made with little or no difficulty. In fact, a primary advantage of the F/S method is that its format simplifies the extrapolation process.

Classical Buckling

Characteristics of the F/S plot in classical buckling situations can be examined by considering the case of a slender column, simply supported at both ends. Consider, first, the case of a column having a small initial curvature, causing an initial lateral displacement δ_0 at the center of the column. The center deflection of the column under application of an end load P is given with good accuracy by

$$\delta = \delta_0/(P_{cr}/P - 1) \tag{1}$$

in which P_{cr} is the classical column buckling load. To examine F/S data obtained from column center deflections, the equation is put in the following form

$$P/\delta = (P_{cr} - P)/\delta_0 \tag{2}$$

From the equation it is seen that a plot of P/δ vs P (the F/S plot) is a straight line of negative slope intersecting the P axis at the classical buckling load P_{cr}. This behavior is illustrated in Fig. 1.

The F/S plot is usually obtained from strain gage data. The bending strain at the center of the column is given by

$$\epsilon_b = kP(\delta + \delta_0) \tag{3}$$

where k is a constant derived from the material and cross-sectional properties of the column. The total center displacement $(\delta + \delta_0)$ is given with good accuracy by

$$(\delta + \delta_0) = \delta_0/(1 - P/P_{cr}) \tag{4}$$

Substituting this into the preceding equation and putting the result into the F/S form we obtain

$$P/\epsilon_b = (1 - P/P_{cr})/k\delta_0 \tag{5}$$

Again, it is seen that the F/S plot, in this case P/ϵ_b vs P is a straight line, intersecting the load axis at the classical buckling load P_{cr}, as in Fig. 1. It should be emphasized that the strain considered here is only the bending strain, such as that obtained from the difference in reading of back-to-back strain gages.

If maximum total strain (i.e., from a single strain gage) is used, the F/S plot loses its linearity. Total strains are given by

$$\epsilon = kP(\delta + \delta_0) + P/AE \tag{6}$$

Substituting from the previous equation for total center displacement into this equation and putting the result in F/S-form gives

$$P/\epsilon = (1 - P(P_{cr})/[k\delta_0 + (1 - P/P_{cr})/AE] \tag{7}$$

The resulting F/S plot is a curve with negative slope, concave downward, which again intersects the load axis at P_{cr}.

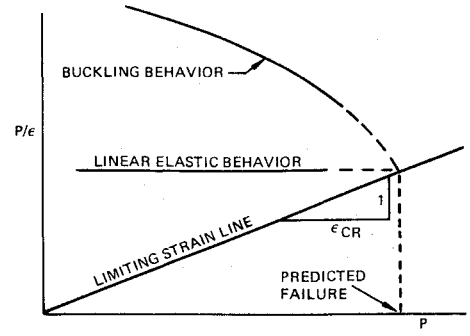

Fig. 2 Limiting strain line on F/S plot.

Another example which is characteristic of many practical test situations is the case of a column with a constant lateral pressure load p subjected to an increasing end load P. The displacement caused by the lateral pressure alone can be considered an initial displacement δ_0. Then, the additional displacement due to application of the end load P is given by Eq. (1). Therefore, the F/S plot [*Eq. (2)*] is linear if the net deflection produced only by the end load is used. Similarly, bending strain may be used [as in Eq. (3) and (5)], to produce a linear F/S plot if it is the net bending strain due to the application of P. Total displacement or total bending strain will produce F/S plots which are curved.

Consideration of these simple examples suggests that, even for complex buckling problems, an F/S plot which is inclined downward to the right (as shown in Fig. 1), is a clear indication of approaching buckling. For buckling which is classical, or is classical in its early stages, the intersection of this line with the horizontal axis, obtained by extrapolation during testing, is an estimate of the general instability load.

Local Failure

The buckling failure of a test specimen is ultimately caused by material failure and/or by a local crippling instability, which renders the specimen incapable of supporting load. Suppose that either analytically or by tests of coupon specimens, a strain level is determined at which local failure will occur. This limiting strain value can be represented conveniently on an F/S plot (as shown in Fig. 2). The limiting strain, denoted by ϵ_{cr}, is represented by a straight line passing through the origin, with inverse slope ϵ_{cr}. In a test of a structure which incorporates parts whose local strength is represented by ϵ_{cr}, failure is indicated by the intersection of the F/S plot with the limiting strain line. Figure 2 illustrates such indicated failure for two types of prefailure behavior: linear elastic behavior and a buckling behavior.

In linear elastic behavior, strain is directly proportional to load; therefore, P/ϵ is constant and the F/S plot is a horizontal straight line. Such behavior might be observed in testing short column specimens where classical general instability is not approached.

In monitoring local failure, it is necessary to use total strain, rather than just the bending component, as in the case of general instability. Therefore, the F/S plot representing buckling behavior is curved, as in the case of Eq. (7), instead of the ideal straight line form of the classical buckling plot. Nevertheless, the plot can usually be extrapolated to its intersection with the limiting strain line to give a reasonably accurate estimate of the local failure load. This approach has proved very valuable for nondestructive local buckling prediction in testing beaded and tubular panels.

When local failure occurs under combined loads, as in the case of a structural panel loaded in compression, shear, and bending, it is necessary to monitor a general biaxial state of strain instead of the simple uniaxial strain considered previously. The strain used in obtaining the F/S plot will then

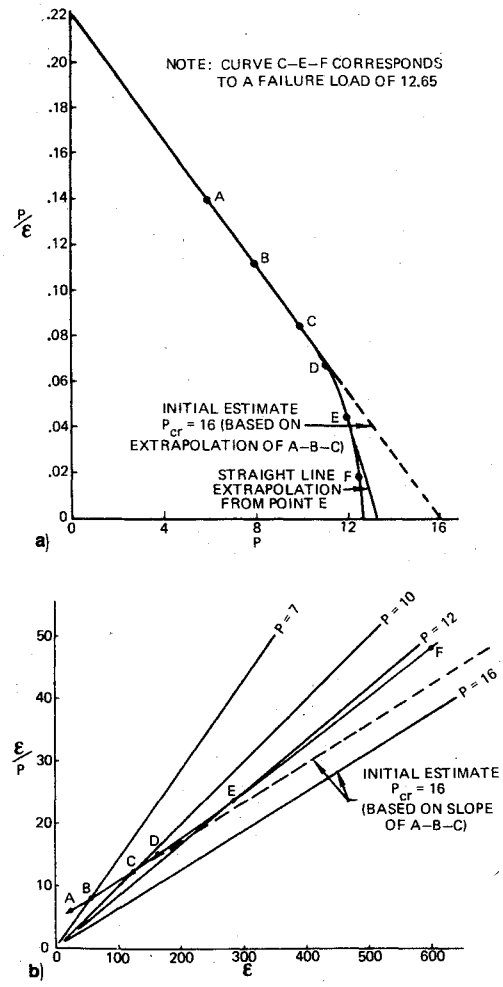

Fig. 3 Comparison of a) *F/S* and b) Southwell plots.

be a generalized strain variable derived from the local failure criteria. For cases in which local failure criteria are expressed in the form of strain interaction equations, the equations themselves provide the definition of the generalized strain variables. This procedure has worked well in practice. For accurate local failure predictions, the interaction equation must be correlated with adequate test data. The test data are normally obtained by destructive testing of material coupons, local buckling specimens, or crippling specimens over the applicable load range. An example showing the use of such a strain interaction criterion is given later in discussing the application of the method to the prediction of local buckling failures in tubular strucctural panels.

Comparison of *F/S* and Southwell Methods

The *F/S* and Southwell methods are equivalent in the sense that they make use of the same basic data and in error-free application would yield the same predictions for buckling loads. It is easily shown that for either method the mathematical form of the failure load prediction P^* in terms of current load P and the current apparent tangent stiffness dP/dD, is‡

$$P^* = P\{(P/D)/[(P/D) - dP/dD]\} \tag{8}$$

where D is a deflection or deformation variable. The corresponding margin to failure during testing is

$$P^* - P = P\{(dP/dD)/[(P/D) - dP/dD]\} \tag{9}$$

‡For the *F/S* method a straight line rather than curved extrapolation is considered here, and the possibility of local buckling is ignored.

Thus, for both methods, an indication of close proximity to failure results from the nearness of the tangent stiffness dP/dD to zero. Though in the mathematical sense the two methods are equivalent, in applications they are not. The actual procedures used are very different, and the quickness and confidence with which buckling load predictions can be made may differ considerably.

Figure 3 shows corresponding *F/S* and Southwell plots for a typical form of test data. Points A through F indicate a chronology of loading on the two plots, and the relative scales have been reproduced accurately. The rays drawn from the origin in the Southwell plot are constant load lines, whose inverse slopes are load values. Thus, at point B, the crossing of the test curve and the $P = 7$ ray indicate that the current load level is 7 units. The failure load estimate is the inverse slope of the plotted curve. At point B it is estimated to be about 16 units by noting that the test curve and the $P = 16$ ray are essentially parallel at this point. In the *F/S* plot, the 7-unit current load level for point B is read on the horizontal plot axis. The failure load is estimated by extrapolation to this axis and again is seen to be about 16 units. The estimate of margin to failure in the Southwell plot is given by the difference between the current inverse slope of the plotted curve, which must be graphically or numerically determined, and the current load value. The corresponding estimate in the *F/S* plot is given by the difference between the extrapolated intersection of the plotted curve with the load axis, and the current load value. In the latter case the margin to failure is read directly on the load axis.

The A to C portions of the plots shown in Fig. 3 are straight. This portion of the data is an important failure indication, in that it is due to a classical instability tendency. This tendency, though often subsequently modified by nonlinear effects, nevertheless usually has a dominant influence on specimen failure load. Subsequent to point C in the figure, the plots are curved. This is a frequently occuring situation, and for such cases it is often necessary to test to relatively high load levels to obtain accurate failure predictions. Thus, the question of what additional load increment can be risked becomes very important. For the example under consideration, the Southwell plot is increasing its slope upward. The test engineer must estimate to which ray the test plot may eventually become tangent (failure condition). In working with slopes and curvatures, particularly when the plot dimensions are rapidly expanding to the right, this is difficult. The difficulty is at least in part a problem of visualization. In the *F/S* plot curvature is handled by simply extrapolating an estimated curved line to the intercept. The extrapolation, being toward an intercept (rather than a slope), and being in a region where the horizontal scale is shrinking rapidly, is easy to visualize. The range of possible failure loads is defined by the region on the load axis between the straight line and the curved line extrapolations. This is indicated in Fig. 3 for point E.

The authors have applied the *F/S* plot to a great many test cases, gaining familiarity with *F/S* plot forms and interpretations and a facility to do the test predictions quickly and with a minimum of indecision. It is their opinion that the *F/S* format, for the reasons outlined and further discussed in the next section, provides a significant application superiority over the Southwell procedure for nondestrictive predictions of complex (nonclassical) buckling phenomena. Typical *F/S* plot forms have been encountered repeatedly, and identified as to characteristic behavior. These are discussed in the next section.

F/S Signatures

A characteristic of the *F/S* method is that important different behavior types display recognizable and physically meaningful signatures when plotted. This is helpful in interpreting data obtained in tests of structures whose buckling behavior is complex or highly nonlinear. Certain of these *F/S*

signatures, which have been encountered frequently, have been identified as to behavior type. They are shown in Fig. 4. The load axis, identified by F in the plots, may represent compression, shear, pressure, or any combination of these which is applied in a constant ratio but varied in magnitude during testing. To identify the stiffness axis it is convenient to use F/D, where D is understood to represent displacement, simple strain, or generalized strain, depending on the application.

Figures 4a and 4b represent the elementary cases of linear elastic and classical buckling behaviors already discussed. Figure 4c shows a case where classical buckling is indicated in the early stages of load application. As the indicated buckling load is approached, nonlinear stiffening causes the slope of the F/S plot to decrease sharply, and it approaches a horizontal tangent. Failure eventually occurs locally due to accumulation of large strains. This is indicated here by intersection of the F/S plot with a limiting strain line. Plots such as this have been found to provide estimates for both the classical buckling load and the failure load. It should be noted that, in practice, the local failure indication is usually obtained from a different set of data than that which indicates general instability, and thus the two estimates are not usually provided by a single plot.

Figure 4d shows typical behavior of two F/S plots, obtained simultaneously from instrumentation in different locations, when a change in buckling mode occurs. In the early stages of loading, one plot shows a clear indication of classical buckling behavior while the other indicates essentially linear elastic behavior. As loading progresses, another mode, which is the critical mode, becomes dominant. At this point, the second F/S plot begins to exhibit pronounced buckling behavior, while the first one curves upward to the right, indicating a regression of the first mode. This behavior has been observed repeatedly in testing beaded and corrugated panels in compression, where the predominant component of initial imperfection is an $n=1$ component, and the critical buckling mode is the $n=2$ component. Buckling loads for both modes are predicted in such cases.

In Fig. 4e, the F/S plot indicates a situation in which bending strain reverses direction as load is increased. This phenomenon usually occurs when initial buckling-type deformations developing in the presence of local imperfections begin to shift to conform to characteristic buckling modes at higher loads. Strain reversal of this type has been observed in compression tests of tubular panels where characteristic square wave buckling patterns develop in the flat elements, and also in testing of externally pressurized ellipsoidal domes. This is the most difficult type of data plot for use in predicting failure. It has been found helpful in such cases to plot absolute rather than signed values.

The F/S plot in Fig. 4f is typical of those often obtained in practice. It differs from the ideal case of Fig. 4b by having some curvature. The curvature is due to principally to the presence of a linear elastic component in the deflectometer or strain gage data. It is difficult to avoid this in complex buckling situations; however, the F/S plot can usually be extrapolated to the load axis without difficulty.

A typical extrapolation of a local instability F/S plot is shown in Fig. 4g. The plot, which is linearly elastic in the early stages of loading, begins to curve downward sharply as buckling behavior begins to influence the load/strain relation. When curvature is pronounced it may be difficult to estimate accurately where the F/S data would intersect the limiting strain line. However, in most cases the distance over which the data are extrapolated is small, resulting in a small probable range in which local buckling failure would be expected. This is the case illustrated. Where curvature makes visual extrapolation of F/S plots difficult, mathematical curve fitting techniques have been used to improve reliability of predictions. To do this successfully, the approximate mathematical form of the F/S plot should be determined and a similar form should be used in the curve fitting routine. Examples of this

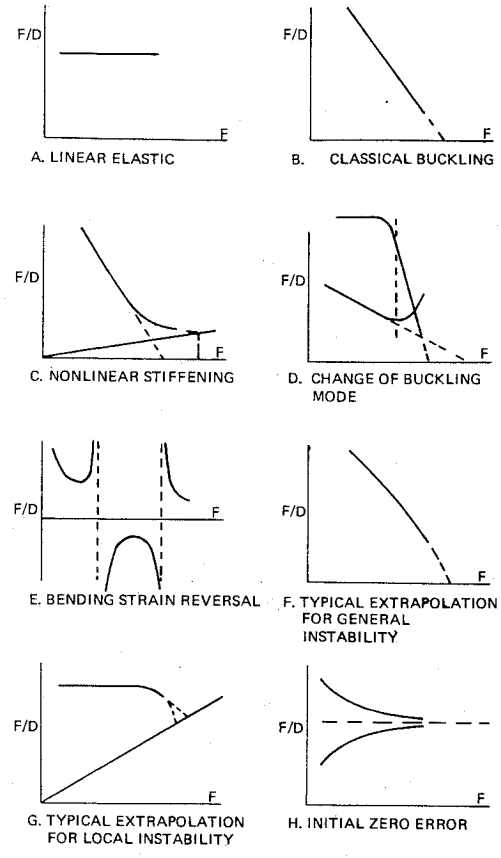

Fig. 4 Typical F/S signatures.

will be shown later. The effect of initial zero error in strain gage or deflectometer readings is illustrated in Fig. 4h for a case of linear elastic behavior.

Applications

Buckling Tests of Beaded and Tubular Panels

Considerable experience in applying the F/S method has been obtained in nondestructive tests of beaded and tubular panel configurations under Contract NAS 1-10749. The test part of this program included testing of ten 40×40-in. full-scale, aluminum structural panels, plus numerous smaller specimens for configuration screening studies and for determining local buckling strengths. The full-scale panels were each tested in 10 different load combinations of axial compression, shear, and lateral pressure to obtain nondestructive failure load predictions. Each of the panels was finally tested to failure in one of the 10 load conditions to verify the F/S failure predictions. Representative test data from this program are presented here. Most of the test data shown are from tests to actual failure, so that the potential accuracy of the method can be seen.

Figures 5-7 present data from configuration screening tests of beaded panels. Each figure includes both general and local instability data. In all cases the local instability strain levels were determined from prior tests of small specimens having the same bead configurations as the full-scale beaded panels. The tests were conducted to failure, with prediction of buckling loads made prior to failure by extrapolation of the F/S plots. These predictions are given by the numbers in parentheses. It is seen that good accuracy could have been obtained in nondestructive testing of these specimens. Figure 5 shows a case where general instability is predicted to occur before local instability. The local instability F/S plot shows linear elastic behavior until immediately prior to the failure, which occurred very nearly at the predicted critical general instability load. The sharp downturn of the local instability

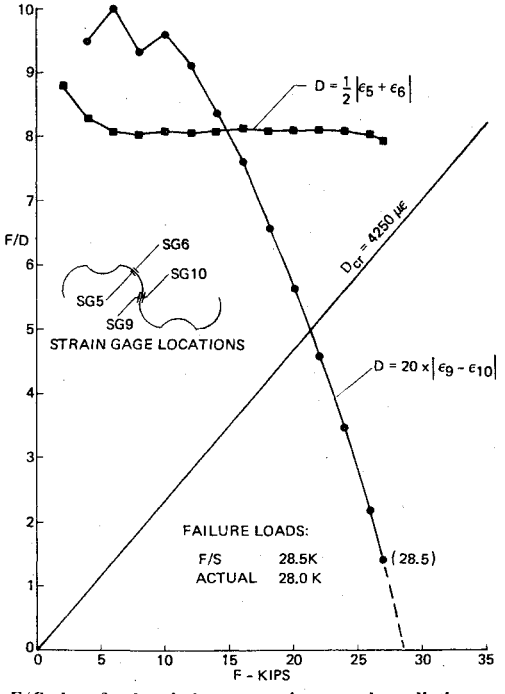

Fig. 5 *F/S* plots for beaded compression panel predicting general instability failure.

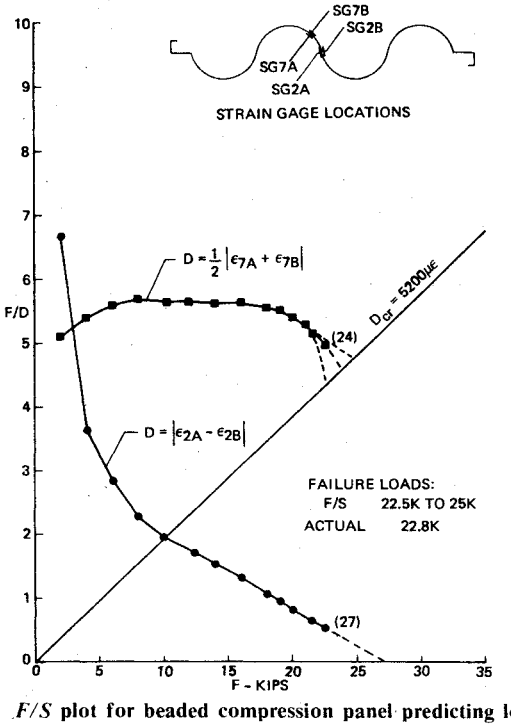

Fig. 7 *F/S* plot for beaded compression panel predicting local instability.

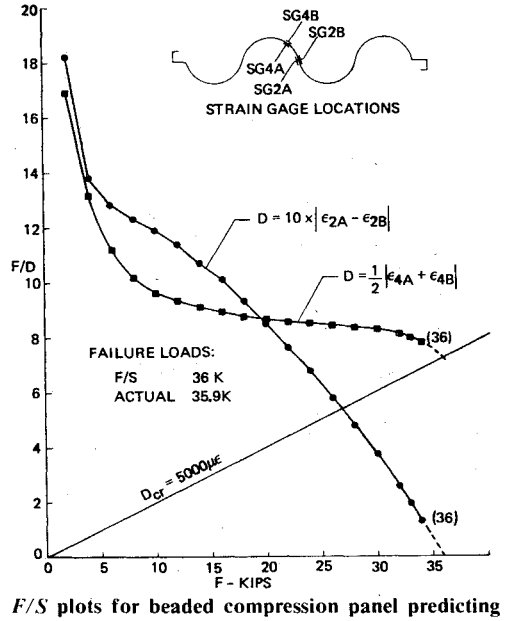

Fig. 6 *F/S* plots for beaded compression panel predicting general and local instabilities occuring at about same load levels.

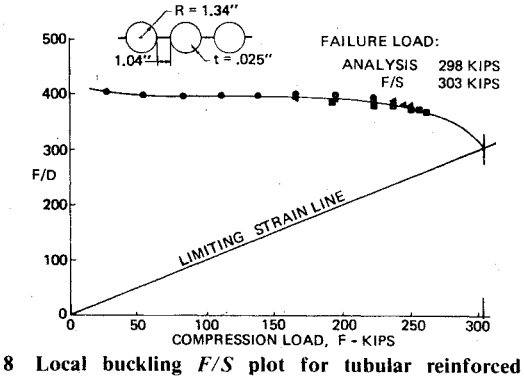

Fig. 8 Local buckling *F/S* plot for tubular reinforced panel-compression only.

curve beginning to show at this point indicates that the specimen is being driven towards a local buckling failure by the onset of the general instability. Figure 6 shows a case where general and local instabilities occur at about the same load levels, and in Figure 7 local instability is predicted with general instability apparently not critical.

Figures 8-10 show typical data from tests of three 40×40-in. tubular panels. Local instability was the critical failure mode for these panels under all conditions of loading. Therefore, the *F/S* plots are of the local failure type. Figure 8 shows a typical nondestructive test where loading was stopped well before indicated failure. Figures 9 and 10 show results of tests to destruction of two of the panels, and are included to show comparisons of the *F/S* indicated failures with the actual failures. Analytical failure predictions are given in all three cases for comparison.

These *F/S* plots were generated using a generalized strain variable *D*, which accounts for axial compression, bending, and shear strain components

$$D=[\epsilon_c/(\epsilon_c)_{cr}]+[\epsilon_b/(\epsilon_b)_{cr}]+(\gamma/\gamma_{cr})^n \tag{10}$$

The critical local buckling strain condition occurs when

$$D=D_{cr}=1 \tag{11}$$

Equations (10) and (11) represent a critical strain interaction surface, which is an extension of the concept of a limiting strain value discussed earlier. This strain interaction surface is the basis for the limiting strain lines shown in Fig. 8-10.

The strain components ϵ_c, ϵ_b, and γ were measured by strain rosettes placed at the outermost fiber on either side of the tube at the panel center. The critical strains $(\epsilon_c)_{cr}$, $(\epsilon_b)_{cr}$, γ_{cr} for compression alone, bending alone, and for shear alone, respectively, and the exponent n were determined analytically. However, the analysis had been modified previously to achieve adequate correlation with local buckling destructive test results over the entire compression-bending-shear load spectrum.

Table 1 Correlation of nondestructive local buckling tests with analysis of 40 × 40-in. tubular aluminum panels

Compression vs shear ratio N_X	N_{XY}	Lateral pressure (psi) P	Correlation factor test/analysis Panel-1	Panel-2	Panel-3
1	0	0	0.97	1.03	0.95
0	1	0	0.99	1.02	1.00
1	1/5	0	1.04	1.17	1.03
1	⅓	0	1.06	1.06	1.04
1	0	1.00	1.21	1.01	1.02
1	0	2.00	1.20	1.05	0.96
0	1	1.00	0.99	1.04	1.01
0	1	2.00	1.02	1.05	0.99
1	1/5	1.00	1.07	1.06	1.03
1	1/5	2.00	0.98	1.08	1.01
		Average	1.053	1.057	1.004

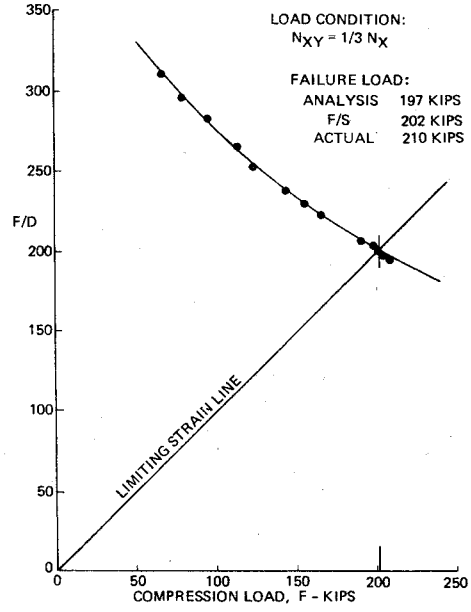

Fig. 9 Local buckling *F/S* plot for tubular reinforced panel-compression + shear.

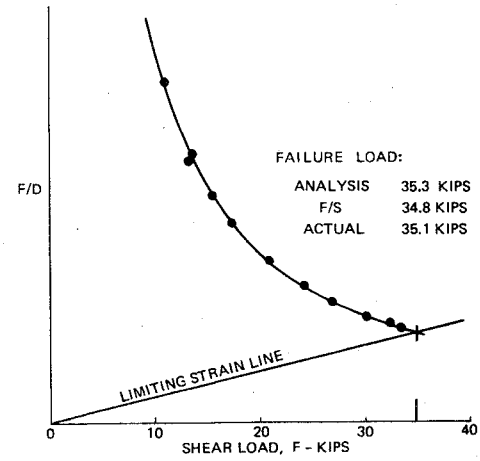

Fig. 10 Local buckling *F/S* plot for tubular reinforced panel-shear only.

Extrapolation of the *F/S* test data to an intersection with the limiting strain line was accomplished mathematically. A library computer routine for performing a least square curve fit was adopted to perform the extrapolation. The mathematical form of the curve used is

$$F(x) = (a_2x^2 + a_1x + a_0) / (b_3x^3 + b_2x_2 + b_1x + b_0) \quad (12)$$

This is the expression available in the routine used which most nearly fits the theoretical form of the local buckling *F/S* data for panels tested in combined axial compression, shear, and lateral pressure. The *F/S* failure load predictions were used to evaluate the accuracy of the analysis procedures developed for the tubular panels. For this purpose three panels of identical design were tested. Table 1 summarizes the correlations achieved.

Externally Pressurized Shells

Experience with the *F/S* method in buckling tests of shells has been very limited. However, the results presented here for two examples show sufficient promise to warrant further investigation of the usefulness of the method in shell buckling testing. This work was done in connection with developing lightweight vacuum jackets for cryogenic insulation, under Contracts NAS3-14369[5] and NAS3-15848, sponsored by NASA Lewis Research Center.

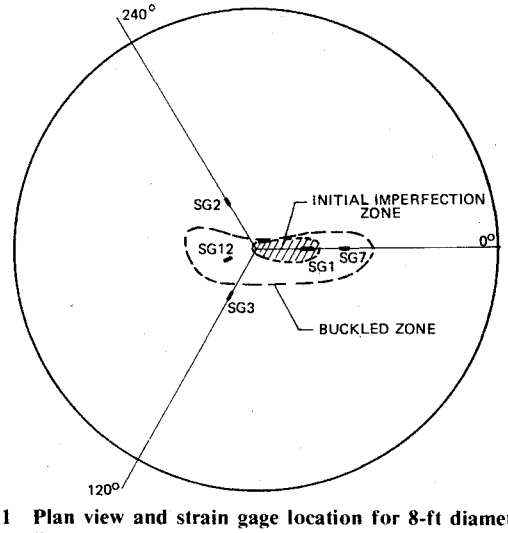

Fig. 11 Plan view and strain gage location for 8-ft diameter ellipsoidal shell.

Figures 11-13 show test data for an externally pressurized, 8-ft diameter, 4:3 ellipsoidal head of laminated sandwich construction. Figure 11 shows a plan view of the ellipsoidal head and the locations of back-to-back strain gage pairs connected to record bending strain. Strain gage pairs 1, 2, and 3 were originally installed in the central region of the head, as shown. In this region a shallow initial imperfection in the form of a slight concavity was observed, which investigation showed to

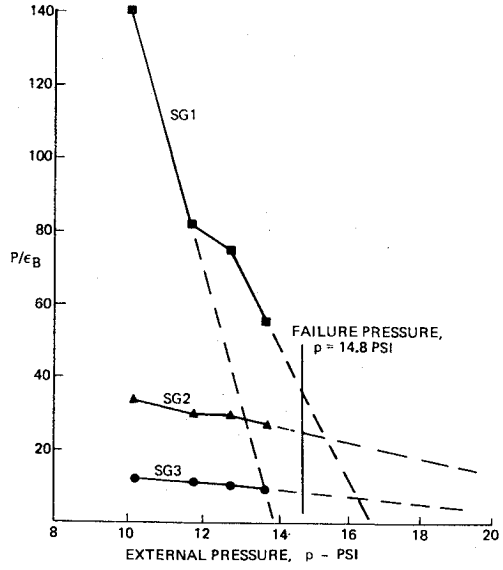

Fig. 12 *F/S* plots for 8-ft ellipsoidal shell.

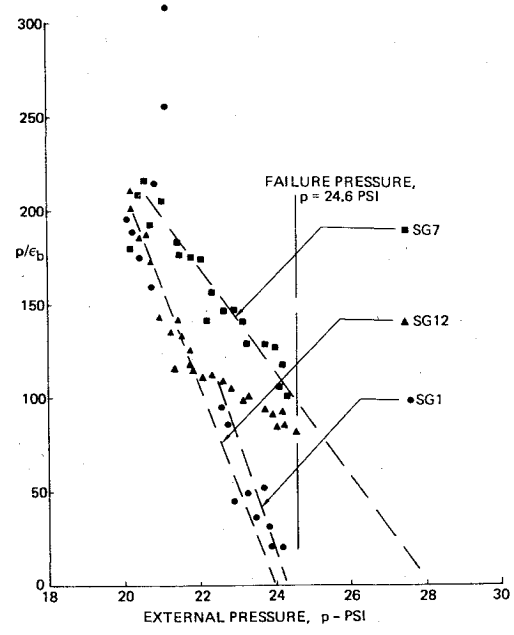

Fig. 13 *F/S* plots for reinforced 8-ft ellipsoidal shell.

be due to the manufacturing process for the inner aluminum shell of the sandwich. Figure 12 shows the *F/S* plots obtained from these three strain gage pairs. Strain gage pair No. 1, which was located nearest the initial imperfection, is the only one showing a buckling indication. General instability is predicted in the range of 14-16.5 psi. Loading was continued until actual buckling occurred at 14.8 psi in the region indicated in Fig. 11.

The loading was by water pressure, so that buckling tended to be controlled and to leave the specimen relatively undamaged. After the first test the buckled region of the shell was repaired and reinforced. Strain gage pairs 7 and 12 were installed to give additional instrumentation in the buckled region, and the shell was retested. Figure 13 shows *F/S* plots from this second test. Data were recorded continuously instead of at discrete intervals, as in the first test. The scatter seen here is probably due to the inelastic influences of the composite sandwich construction materials (i.e., fiberglass, resin, and bonding agent). Below 20 psi the bending strains were small and no buckling indication was observed. Above

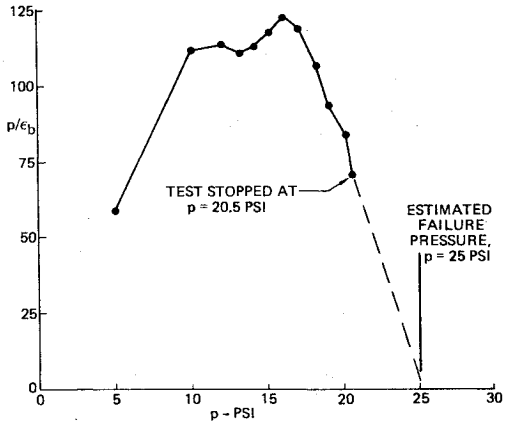

Fig. 14 *F/S* plots for 100-in. hemispherical shell.

20 psi strain gage pairs 7 and 12 show fairly clear indications of buckling occuring at 28 psi and 24 psi, respectively. Above 22 psi strain gage pair no. 12 shows typical nonlinear stiffening behavior. Strain gage pair no. 1 showed two strain reversals occurring between 21 and 22 psi. Above 22 psi the *F/S* plot descended rapidly, eventually indicating buckling at about 24 psi. Actual buckling, accompanied by catastrophic failure, occured at 24.6 psi.

The buckling testing of the ellipsoidal pressure head was a difficult application of the method and it is doubtful that these data could have been used with much confidence in determining accurate buckling loads nondestructively. However, these tests showed sufficient promise to warrant the further use of the method in proof testing a 100-in. diameter, hemispherical, vacuum jacket, of aluminum sandwich construction, with external pressure. The purpose of using the *F/S* method in this test was to monitor the approach to buckling so as to avoid inadvertent failure of the shell. *F/S* data were monitored from 28 pairs of back-to-back strain gages which were located on the shell after a study of analytical mode shapes and the initial imperfections of the shell due to manufacturing processes. The gages were placed at intervals along meridians spaced 30 to 60 deg apart. The majority of the gages were within a circle located 24 in. meridionally from the apex, with additional gages placed at intervals on selected meridians down to a girth ring located 84 in. meridionally from the apex. Figure 14 shows *F/S* data from the strain gage pair indicating the lowest buckling load. This pair of gages was located 17 in. meriodionally from the apex of the shell. The test was stopped at 20.5 psi, which was sufficient to demonstrate an adequate margin of safety for the design working pressure of 14.7 psi. The critical buckling pressure was estimated by extrapolation to be about 25 psi.

Conclusions

While considerable material has been published on nondestructive buckling testing, the *F/S* format is believed to be an improved concept. The method described has been found in many tests to provide accurate predictions of buckling strengths. It has been able to distinguish between general and local failure and to provide both types of strength predictions in a single test. In addition, the method is conveniently and rapidly used during actual testing. It should not be assumed that any nondestructive test method will always be accurate and reliable for such a complex phenomenon as buckling. Therefore, it is suggested that the procedure be used with an understanding of its approximate nature, and with the expectation that further experience will provide improved accuracy and reliability.

The method relies on the availability of a great deal of data for cases of complex buckling behavior. Many strain gage channels usually will be required to monitor all locations of a

structure at which local buckling may occur or which are likely to be highly deformed by different general instability mode shapes. Automatic data processing during testing is helpful in obtaining maximum utility from the method. Direct F/D vs F readout, or plotting, for both uniaxial and bending strain, is almost mandatory if many data channels are used. This permits quick scanning of all F/S plots, identification of those which describe imminent buckling behavior, and estimation of the buckling load and type of mode involved.

References

[1]Galletly, G.D. and Reynolds, R.E., "A Simple Extension of Southwell's Method for Determining the Elastic General Instability Pressure of Ring-Stiffened Cylinders Subject to External Pressure," *SESA Proceedings*, Vol. XII, No. 2, 1955, pp. 141-152.

[2]Datta, P.K. and Carlson, R.L., "Buckling and Vibration of a Thin Tensioned Sheet with an Elliptical Hole," Experimental Mechanics, Vol. 13, July 1973, pp. 280-286.

[3]Craig, J.I. and Duggan, M.F., "Nondestructive Shell Stability Estimation by a Combined Loading Technique," *Experimental Mechanics*, Vol. 13, Sept. 1973, pp. 381-388.

[4]Musgrave, M.D. et al., "Advanced Beaded and Tubular Structural Panels," *Journal of Aircraft*, Vol. 11, Feb. 1974, pp. 68-75.

[5]Barclay, D.L. et al, "Lightweight Evacuated Multilayer Installation Systems for the Space Shuttle Vehicle," NASA CR121105, May 1973.